# INVESTIGATION OF NOVEL SOLID OXIDE FUEL CELL CATHODES BASED ON IMPREGNATION OF $SrTi_xFe_{1-x}O_{3-\delta}$ INTO CERIA-BASED BACKBONES

M. Brinch-Larsen, M. Søgaard, J. Hjelm and H. L. Frandsen
Fuel Cells and Solid State Chemistry Division, Risø National Laboratory for Sustainable Energy, Technical University of Denmark (Risoe DTU), DK-4000 Roskilde, Denmark



## ABSTRACT

Solid oxide fuel cell (SOFC) cathodes were prepared by impregnating the nitrates corresponding to $SrTi_xFe_{1-x}O_{3-\delta}$ (STF), x = 0; 0.1; 0.2; 0.3; 0.4 and 0.5, into a porous backbone of $Ce_{0.9}Gd_{0.1}O_{2-\delta}$ (CGO). STF was chosen as very high oxygen surface exchange rate, high ionic conductivity and electrochemical stability as a thin film electrode have been reported for these materials. XRD measurements showed a high degree of secondary phase formation in the infiltrate as well as reaction with the CGO backbone. Microstructural analysis showed that the STF infiltrate had formed a coating on the CGO backbone. All prepared electrodes were characterized as symmetric cells using impedance spectroscopy. Within the investigated series the infiltrate with x = 0.1 (STF10) showed the best performance with an area specific resistance (ASR) of ASR ≈ 6.4 Ω cm$^2$ (STF10) at 600 °C in air. The relatively poor performance is believed to originate from poor electronic conduction in the electrodes and possibly also reactions between Sr-containing compounds and CGO. To circumvent the low electronic conductivity, backbones of a composite cathode containing $LaCo_{0.4}Ni_{0.6}O_{3-\delta}$ (LCN60) and CGO were also tried infiltrated with STF. The ASR of the backbone was 8.7 Ω cm$^2$ prior to infiltration and this decreased to 0.34 Ω cm$^2$ after infiltration with STF10.

## INTRODUCTION

Rising prizes of fossil fuels and the urge for reducing the global warming call for sustainable and efficient technologies for conversion of chemical energy into electricity and heat. Solid oxide fuel cells (SOFCs) could potentially contribute to a global energy solution. But a number of critical issues need to be resolved before significant commercialization can take place. Issues that must be solved are among others high material costs and high degradation rates. Extensive research of new potential materials is therefore needed for the success of the technology.

In the search for new cathode materials for SOFCs perovskites in the series $SrTi_xFe_{1-x}O_{3-\delta}$ (STF) could be interesting since thin film electrodes of the material have shown a performance superior to that of the commonly used $La_{0.6}Sr_{0.4}Co_{0.2}Fe_{0.8}O_{3-\delta}$ (LSCF). Oxygen exchange rates in the range of k = $1.2\text{-}2.0 \cdot 10^{-5}$ cm/s at 800 °C have been reported for compositions x = 0.50-0.95 (STF50-STF95). It is thus expected that the compositions x = 0-0.50 also possess high exchange rates. The purpose of this work is to further evaluate the potential of using STF materials through fabrication and test of porous SOFC cathodes [1].

Previous studies have shown that the bulk electronic ($\sigma_e$) and ionic ($\sigma_i$) conductivities of STF both increase with increasing iron content throughout the entire compositional range $SrTi_xFe_{1-x}O_{3-\delta}$, x = 0-0.99. For $SrFeO_{3-\delta}$ (STF00) $\sigma_e$ = 20-35 S/cm and $\sigma_i$ = 0.21 S/cm, whereas for $SrTi_{0.5}Fe_{0.5}O_{3-\delta}$ (STF50) the conductivities $\sigma_e$ = 1.0 S/cm and $\sigma_i$ = 0.05 S/cm have been measured at 850 °C in air [2,3]. The electronic conductivity of STF at 850 °C is thus 1-2 orders of magnitude lower than the electronic conductivity for LSCF of $\sigma_e$ = 300 S/cm, whereas the ionic conductivity of STF is significantly larger than that of LSCF at 850 °C, $\sigma_i$ = 0.015 S/cm [4].

The thermal expansion coefficient (TEC) of STF increases with increasing content of iron. In the temperature regime ~500-800 °C values of $22 \cdot 10^{-6}$ $K^{-1}$ and $27 \cdot 10^{-6}$ $K^{-1}$ have been reported for $SrTi_{0.05}Fe_{0.95}O_{3-\delta}$ and $Sr_{0.97}Ti_{0.20}Fe_{0.80}O_{3-\delta}$, respectively [5,6]. The ratio of these values is not as expected from the respective compositions. They must thus be attributed some uncertainty. For lower contents of iron values of $17 \cdot 10^{-6}$ $K^{-1}$ and $9 \cdot 10^{-6}$ $K^{-1}$ have been measured for $Sr_{0.97}Ti_{0.4}Fe_{0.6}O_{3-\delta}$ and $SrTiO_3$, respectively [6,7]. The TEC for Fe rich STF compositions is thus much larger than that of usual SOFC components, ~$11 \cdot 10^{-6}$ $K^{-1}$ [8], which may cause problems in composite electrode designs.

The need for screening the potential of various STF compositions as cathode materials in a feasible electrode design calls for quick fabrication techniques. It was chosen to fabricate and characterize impregnated electrodes. Hence, an aqueous solution of the nitrates corresponding to STF was introduced into an already physically and chemically stable ionic conducting backbone. The impregnated cell design diminishes the importance of matching the TEC of STF to that of other cell components and allows us to use Fe rich STF compositions without complications. Impregnated electrodes have previously shown excellent performance by impregnation of nitrates corresponding to $La_{0.6}Sr_{0.4}CoO_{3-\delta}$ (LSC40) and $Sm_{0.5}Sr_{0.5}CoO_{3-\delta}$ into backbones of $Ce_{0.9}Gd_{0.1}O_{3-\delta}$ (CGO) [9,10].

In this work the possibility of using STF impregnated porous SOFC cathodes is tested and the most suitable composition is found. STF with compositions x= 0-0.5 are characterized with respect to electrochemical performance, phase formation and microstructure. The high contents of Fe have been chosen in order to get high electronic and ionic conductivities, which is desirable in SOFC electrodes.

Two types of backbones have been investigated for the potential of impregnating STF. A backbone of CGO was tried first. This backbone has a very high ionic conductivity and almost no activity towards oxygen reduction. In a second round, backbones of $LaCo_{0.4}Ni_{0.6}O_{3-\delta}$/CGO (LCN60/CGO) were used. LCN60 has a high electrical conductivity, 1200-1500 S/cm at 25-1000 °C in air, but also a low ionic conductivity as vacancy formation only takes place at high temperature. Although LCN60 itself works as an oxygen reduction catalyst, it was expected that the electrode performance could be improved through impregnation. [11]

## EXPERIMENTAL

### Preparation of Cells

Symmetric 5 x 5 $mm^2$ cells with CGO electrode backbones were prepared by screen printing on each side of a 300 µm thick commercial $Ce_{0.9}Gd_{0.1}O_{3-\delta}$ (CGO) electrolyte and subsequently sintering at 1150 °C. The CGO backbones had a porosity of 64 % and a thickness of 30 µm on one side and 45 µm on the other [9]. The differences were due to the screen printing procedure and are not expected to influence the electrode performance, since the electrochemical reaction zones are primarily located within a few tens of micrometers of the electrolyte/cathode interface. The electrode backbones were impregnated with aqueous precursor solutions consisting of a surfactant, strontium nitrate $Sr(NO_3)_2$, iron nitrate $Fe(NO_3)3 \cdot 9H_2O$ and titanium lactate $C_{12}H_{20}O_{12}Ti$ in amounts corresponding to $SrTi_xFe_{1-x}O_{3-\delta}$, x= 0; 0.1; 0.2; 0.3; 0.4; 0.5.

The CGO electrode backbones were impregnated according to the procedure illustrated in Figure 1a; (i) – (ii) the porous backbone was impregnated by placing a drop of precursor solution onto the cell and any surplus precursor solution was removed using a tissue; (ii) - (iii) the solvent was evaporated and the surfactant was decomposed by pre-heating in an oven at 350 °C for 15 min. Any leftover infiltrate on the surface of the electrodes was removed, after which a new infiltration followed. This procedure was repeated 14 times.

The amount of infiltrated material was measured by weighing the cells before and after impregnation. Since formation of phase pure STF cannot be expected after calcination at only 350 °C, thermogravimetry of the pre-calcined STF powder was carried out up to a temperature of 1000 °C. Weight losses in the range of 29-36 % resulted from decomposition of the pre-calcined powder.

Subtracting this weight loss and assuming complete formation of STF the resulting volumetric percentage of infiltrated material in the electrode backbones was estimated to 15 % (STF00, density $\rho$ = 5.26 g cm$^{-3}$) and 17 % (STF50, $\rho$ = 5.15 g cm$^{-3}$) of the total electrode volume, including pores and backbone. Densities were calculated from molar masses of the constituent elements and unit cell parameters [5].

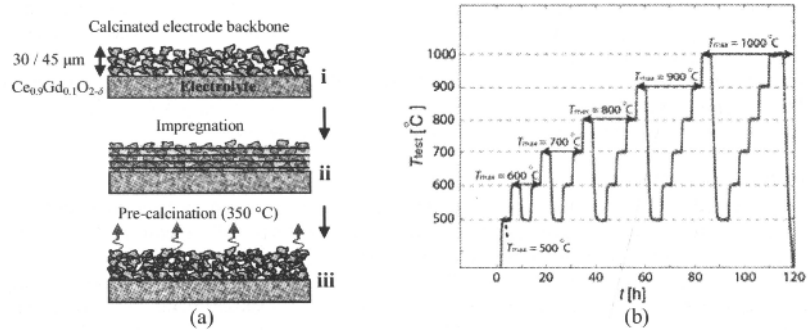


Figure 1. (a) The impregnation procedure starting with a sintered electrode backbone on top of an electrolyte. The backbone was impregnated with a precursor solution and pre-calcined at 350 °C. The last step was followed by a new impregnation. (b) Temperature cycle during symmetric cell characterization. The cells were tested at various temperatures ($T_{test}$) after different calcination temperatures ($T_{max}$). The arrows show the $T_{max}$ periods of the test.

Symmetric cells with 5 x 5 mm$^2$ LCN60/CGO 50/50 wt% electrode backbones were impregnated as well. The LCN60/CGO symmetric cells were electrolyte supported by a 200 µm thick CGO electrolyte. The fabrication of these electrodes is described elsewhere [11]. Electrode thicknesses varied between 45-55 µm on one side and 70-85 µm on the other.

The LCN60/CGO backbones were impregnated with the most suitable infiltrate based on the findings from the backbones consisting of CGO, which was found to be STF10. The number of impregnations along with the impregnation procedure was slightly varied for some of the impregnation cycles compared to the impregnation of pure CGO backbones. This was done by increasing the amount of surplus precursor solution left on the cells and by leaving the cells in a vacuum chamber at a pressure of ~ 1 mbar for 5 min, prior to pre-calcination. The vacuum step removes air in the backbone pores and increases the penetration of the precursor solution into the pores [9]. The number of impregnations was varied to optimize the cell performance, and the abovementioned modifications of the impregnation procedure were carried out in order to optimize the amount of infiltrate left in the backbone after each impregnation cycle.

Electrochemical Characterization

The symmetric cells with infiltrate were contacted with Pt paste from Ferro and impedance measurements with in-situ sintering of the infiltrate were carried out using a Hioki impedance analyzer with a frequency range from 0.06 Hz to 100 kHz or a Solartron 1260 impedance analyzer with a frequency range from 0.06 Hz to 1 MHz. The impedance was measured with 15-20 points per frequency decade.

The measurements were carried out on 4 cells at a time at an air flow of 6 NL/h using the temperature cycle shown in Figure 1b. This temperature cycle was applied in order to test the symmetric cells at different temperatures ($T_{test}$) and after different calcination temperatures ($T_{max}$).

Initially the cells were sintered at 500 °C for 120 min. and the impedance was measured for one cell at a time. This procedure was repeated at every temperature plateau. The temperature was then increased to the temperature plateau at $T_{max}$ = 600 °C at a rate of 300 °C/h and ramped back down to 500 °C. This procedure was repeated up to temperature plateaus at $T_{max}$ = 700 °C, 800 °C, 900 °C and 1000 °C with a temperature plateau at every 100 °C while ramping up the temperature, whereas the temperature was ramped directly down to 500 °C after each $T_{max}$ plateau. The temperature cycle gives the possibility of comparing the impedance for a cell sintered at a certain $T_{max}$ at various test temperatures $T_{test} \leq T_{max}$, and furthermore the impedance variation with sintering temperature can be followed by comparing measurements recorded at a certain $T_{test}$ but with varying $T_{max}$. Some tests were carried out up to 900 °C only, since strong degradation of the performance was observed above this temperature. Impedance results were normalized to the cell areas and divided by two.

Characterization of Microstructure and Phase Purity

Impregnated cells sintered at relevant temperatures were fractured by hand and contacted with carbon tape as preparation for scanning electron microscopy (SEM). SEM measurements were carried out using a Zeiss Supra 35 scanning electron microscope.

A precursor solution of STF00 and STF50 was heated to 350 °C for 7 h and subsequently crushed. High-temperature X-ray powder diffraction (HT-XRD) measurements that allows for in-situ calcination were carried out using a Bruker D8 Bragg-Brentano diffractometer with Cu Kα radiation to verify the formation of the STF phase and to study the formation of other phases in the dried precursor solutions. Measurements were recorded for the compositions STF50 and STF00 to retrieve information about the two end members studied in this work. The temperature was varied from 500-900 °C using a Pt heater, heated by Joule heat. Measurements were recorded at every 100 °C. The powder was calcined for 1.5 h (STF50) or 3 h (STF00) at the respective temperature before measuring in order to mimic the sintering times of the symmetric cells before the impedance measurements. Measurements could only be recorded for relatively small amounts of powder at a time, approximately 200 mg. The $2\theta$ range was 17-80 ° with a step size of 0.06 °, and the measurement time per point was 5 s.

The possibility of reactions between STF and CGO was studied using XRD powder diffraction on powder mixtures calcined at 1100 °C for 10 h. Powder mixtures consisted of CGO powder with a surface area of 6.0 $m^2/g$ mixed with dried STF50 and STF00 powder, respectively.

## RESULTS AND DISCUSSION

Phase Evolution and Microstructure as Function of Temperature

The results of the HT-XRD are shown in Figure 2a (STF50) and Figure 2b (STF00). The lower XRD pattern in both figures shows a measurement recorded at 30 °C of the powder of the precursor solution heated to 350 °C. Above it is shown patterns recorded at the temperature stated to the right in the figures. The measurement marked as 30 °C* has been measured at 30 °C after cool down from calcination at 900 °C. At higher temperatures the peaks move towards lower Bragg angles due to lattice expansion. Some measurements have been excluded for both powders, since no change in peak intensity could be observed.

From the HT-XRD patterns for the STF50 powder in Figure 2a it is observed that the only clearly detected phases after calcination at 350 °C are those of the Pt-heater (■ identified as PDF no. 00-004-0802), $Sr(NO_3)_2$ (♣ PDF no. 00-025-0746) and $SrCO_3$ (▼ PDF no. 01-084-1778). $Sr(NO_3)_2$ is not observed at a sintering temperature of 500 °C and above. In contrast, previously observed decomposition temperatures of $Sr(NO_3)_2$ are in the range of 550-620 °C [12,13]. This discrepancy may be attributed to uncertainties on the temperature of the Pt heater and the influence of other present phases on the decomposition and formation temperatures. $SrCO_3$ is observed in all the recorded measurements. However, the peaks of the $SrCO_3$ phase appear only weakly at 350 °C and decrease

significantly when heating to 900 °C. In a similar experiment performed on a dried precursor solution of La, Sr and Co nitrates the $SrCO_3$ was undetectable at 900 °C and above. This discrepancy is believed to be due to a lower stability of STF compared to the formation of $La_{0.6}Sr_{0.4}CoO_{3-\delta}$ (LSC40) in the temperature range 500-900 °C [9].

In Figure 2a the STF50 phase (♦ identified as $SrTi_{0.5}Fe_{0.5}O_{2.85}$ PDF no. 01-084-1004) appears, although only weakly, at 500 °C, but the peaks increase significantly when heating to 700 °C and 900 °C showing increased but not complete formation of this phase. The exact oxygen non-stoiciometry of the phase is not known, since the XRD patterns of various non-stoichiometries are almost identical. It should be mentioned that the XRD peaks of the isolating $SrTiO_3$ phase are located at almost the exact same Bragg angles as the STF50 phase. The unwanted $SrTiO_3$ may thus be present, although further investigation would have to be carried out to reveal the presence of the phase as well as the exact amount. Cooling down from 900 °C to 30 °C a SrO phase (● PDF no. 00-048-1477) appears.

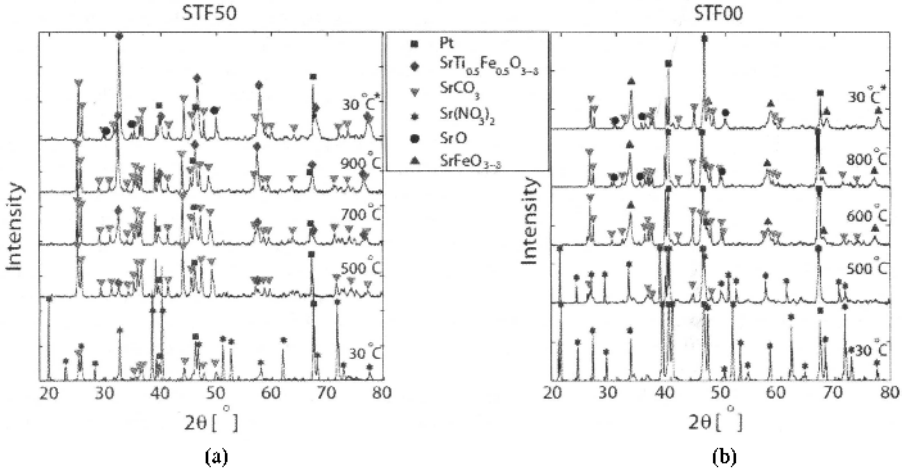


Figure 2. HT-XRD patterns for precursor solution powders of (a) STF50 and (b) STF00. The patterns noted as 30 °C, shown in the bottom of both figures, were recorded after drying at 350 °C, whereas the patterns in the top (30 °C*) were recorded after calcination at 900 °C.

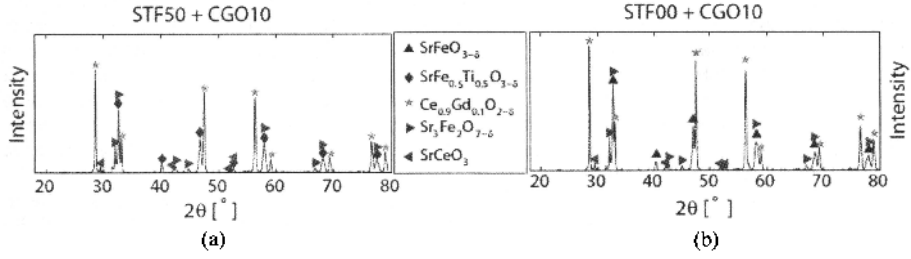


Figure 3. XRD patterns of (a) STF50 + CGO and (b) STF00 + CGO powder mixtures after calcination at 1100 °C for 10 h.

The observed secondary phases do not include iron nor titanium, which must thus be present as additional secondary phases. It has been attempted to match the XRD patterns with the full range of compunds containing either Fe, Ti, Sr, O, C or N but none of these phases were detectable.

The HT-XRD measurements for the STF50 powder thus point at formation of the STF50 phase increasing continuous and strongly between the temperatures 500-900 °C. Furthermore, the XRD data clearly indicate the presence of several unwanted secondary phases. Further investigations are required to reveal the exact amount of secondary phases and STF, respectively. However, comparison with other studies indicates a large presence of $SrCO_3$ in the STF infiltrate and thus a weaker presence of the perovskite phase [9].

The HT-XRD pattern for STF00 is shown in Figure 2b. The $Sr(NO_3)_2$ phase (*) is again observed after heating to 350 °C and is, as in the case of the STF00 dried powder still present after sintering at 500 °C unlike for the STF50 powder. The $SrCO_3$ phase (*) is first observed at 500 °C, however the peaks appear only weakly below 600 °C. The phase is still observed after sintering at 900 °C like for the STF00 powder. The STF00 phase (▲ identified as $SrFeO_{2.73}$, orthorhombic, PDF no. 00-040-0906) is first clearly observed at 600 °C. The peak signals from STF00 appear to increase only weakly with increasing temperature. Further phase formation is expected at a temperature above 900 °C. However, as expected the presence of the poorly conducting, ordered brownmillerite phase, $SrFeO_{2.5}$ can be excluded [2,14].

XRD diffraction patterns for mixtures of CGO with STF00 and STF50, which have been calcined at 1100 °C, are shown in Figure 3. The CGO phase (☆ identified as $Ce_{0.9}Gd_{0.1}O_{1.95}$ PDF no. 01-075-0161) is clearly observable in both powder compositions. Furthermore STF50 (♦ identified as $SrTi_{0.5}Fe_{0.5}O_{2.88}$ PDF no. 01-081-0685) and STF00 (▲ identified as $SrFeO_{2.86}$, tetragonal, PDF no. 00-039-0954) phases are observed from Figure 3a and Figure 3b, respectively. The secondary phases observed at 500-900 °C are not observable after calcination at 1100 °C. However, new peaks have appeared; $Sr_3Fe_2O_{7-\delta}$ (► identified as $Sr_3Fe_2O_{6.75}$ PDF no. 00-045-0400) and a weak trace of $SrCeO_3$ ( ◄ PDF no. 00-047-1689), are observed for both powder mixtures. The $Sr_3Fe_2O_{7-\delta}$ phase has previously been observed in various synthesis methods of strontium ferrite after powder calcinations at 600 °C and 1100 °C and has been shown to decompose again after heating for 100 h at 1100 °C [15]. The formed $SrCeO_3$ phase is a stable, electrically insulating perovskite and is highly unwanted as a secondary phase [16]. It is a product of reactions between $SrCO_3$ and $CeO_2$ and forms at temperatures above 700 °C [17]. This shows that a reaction takes place between the backbone and the infiltrate.

Micrographs showing representative microstructues of a non-impregnated CGO backbone and impregnated CGO backbones are shown in Figure 4. The porous backbone without infiltrate in Figure 4a shows particle sizes in the range 100-300 nm. The infiltrate is clearly observed as small particles of sizes below 20 nm in the STF50 impregnated backbone sintered at 600 °C (Figure 4b). The infiltrate particles appear to be interconnected, which is important for electronic conduction. To some degree the infiltrate also appears to form a thin coating of the CGO particles. and the two components seem to form a good contact. Sintering at 1000 °C implies increased particle sizes of the infiltrate and thus a decrease of the amount of triple phase boundary (TPB), e.g. reduced reaction area, see Figure 4c. After sintering at 1000 °C the STF50 infiltrate is hardly distinguished from the backbone, but it is believed to appear as particles with sizes below 100 nm. The contact angle between the backbone and infiltrate phases appears to be very small, and from the XRD investigations the particles are likely to have reacted with the backbone, forming $SrCeO_3$.

The STF00 infiltrate was significantly harder to detect, although the weight increase due to infiltrated material showed almost equal amounts of infiltrated material of STF00 and STF50. A CGO backbone with STF00 infiltrate sintered at 600 °C is shown in Figure 4d. It is believed that the STF00 impregnated electrodes contain in the vicinity of 15 vol% as calculated from the weight increase due to impregnation. The infiltrate is partly present as clearly observable agglomerates as shown in Figure 4d

and a hardly observable thin coating of the backbone particles. The coating appears as small roughness features on the otherwise smooth backbone particles and edges of the coating have been observed. It is preferable that the infiltrate forms a lot of smaller particles instead of the coating in order to maximize the available surface area for oxygen reduction.

The morphological differences between the STF00 and STF50 infiltrates are attributed to a higher sinterability and possibly higher mobility on the CGO backbone of the STF00 particles. The formation of an infiltrate coating has previously been observed for other perovskites on a YSZ backbone [18,19]. The tendency of the STF00 infiltrate to coat the backbone is further evidenced in Figure 4e, where the STF00 infiltrate has been sintered at 1000 °C and does not appear as individual particles unlike the STF50 infiltrate.

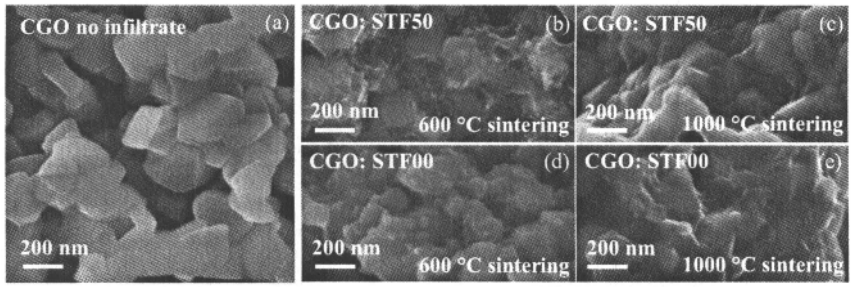


Figure 4. SEM micrographs of CGO backbones with (a) no infiltrate, (b) + (c) STF50 infiltrate calcinated at 600 °C (b) and 1000 °C (c) and (d) + (e) STF00 infiltrate calcinated at 600 °C (d) and 1000 °C (e).

Effect of STF Composition on Electrode Performance

Figure 5a shows Nyquist plots of impedance data from symmetric CGO cells infiltrated with the six investigated compositions $SrTi_xFe_{1-x}O_{3-\delta}$, x= 0, 0.1, 0.2, 0.3, 0.4, 0.5. The cells have been tested in air at $T_{test}$ = 600 °C after in-situ sintering at $T_{max}$ = 600 °C. The insert is a zoom-in of the data for the cells infiltrated with STF00 and STF10. A trend is clearly observed; the data for the STF50 impregnated cell have the highest impedance, and the total area specific resistance (ASR) is decreasing with increasing content of iron. This tendency corresponds to the increase in $\sigma_e$ and $\sigma_i$ with increasing amount of Fe in the composition but is also influenced by the differences in microstructure and the amount of perovskite phase present for different STF compositions as elaborated below. The cells infiltrated with STF00 and STF10 appear to perform almost equally well at $T_{test} = T_{max}$ = 600 °C. Including other sintering and test temperatures, the STF10 infiltrated cells generally perform the best at 500 °C < $T_{test}$ < 750 °C, while the STF00 cells perform better at 750 °C < $T_{test}$ < 1000 °C.

The data in Figure 5a show two clearly distinguishable impedance arcs, which both decrease systematically in magnitude with increasing Fe content of the infiltrate. The low frequency (LF) arc is attributed to a convolution of low frequency electrode processes, which are dominated by the electrochemical reduction of oxygen and the migration of oxide ions between the electrode reaction zones and the electrolyte. The LF arcs show very high impedances of $R_{LF} \approx$ 1.5-15 Ω cm$^2$ in comparison to similar previous studies for CGO backbones impregnated with LSC40, where a polarization resistance of $R_p$ = 0.04 Ω cm$^2$ has been reported at 600 °C in air [9]. Hence, the LF electrode processes must be strongly impeded in the STF impregnated electrodes. The impediment of the LF processes are mainly explained by the widespread formation of secondary phases and insufficient

phase formation of STF, since it is not expected that any of the observed secondary phases can replace neither the ionic and electronic conductivity nor the catalytic activity of the perovskite.

From the SEM investigations the infiltrate particles are expected to be sufficiently interconnected for electron transport to the TPB (reaction zone). However, a combination of a low electronic conductivity and insufficient phase formation of STF may impede the electronic and to some degree also the ionic conduction in the electrode. $SrCeO_3$ that results from reaction of the infiltrate with the backbone is a very poor conductor with a total conductivity of $1.6 \cdot 10^{-4}$ S/cm at 850 °C in air, and may thus cause a significant impediment of the transport of oxide ions from the reaction zone on the STF infiltrate to the CGO phase [16]. Previous studies did not detect the $SrCeO_3$ phase below 700 °C [17]. However, it is not unlikely that the phase is present in minor amounts. Formation of a few nanometers of the phase at the backbone-infiltrate interface would be fatal for the electrode performance because of the low conductivity of the phase.

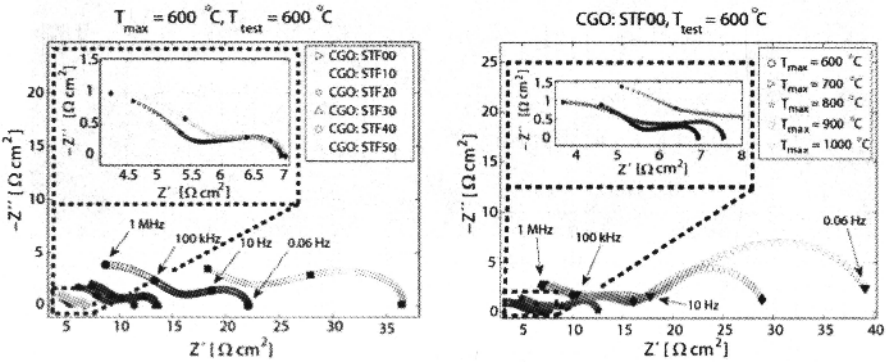


Figure 5. Nyquist plots of impedance data obtained for impregnated symmetric CGO backbone cells in air. (a) Comparison of STF compositions. (b) Comparison of in-situ sintering temperatures ($T_{max}$) for $SrFeO_{3-\delta}$ (STF00). Characteristic frequencies of 0.06 Hz, 10 Hz, 100 kHz and 1 MHz marked.

The HF arc shown in the plots in Figure 5a are observed at unusual high frequencies (~ 1MHz), at which MIEC cathode electrode processes are not normally observed. The HF arc cannot be due to the electrolyte nor the backbone, as it has been observed even at $T_{test}$ = 800 °C and varies in magnitude with STF composition. The high frequency processes can be caused by either low electronic conductivity in the electrode or formation of the $SrCeO_3$ phase. Widespread presence of non-conductive secondary phases in the infiltrate will lower the net electronic conductivity and may also partly disconnect the electronic percolation in the electrode. Formation of the $SrCeO_3$ at the infiltrate-backbone interface will also lead to a HF-process in the impedance spectra.

It is associated with a significant uncertainty to determine series and polarization resistances of the symmetric cells due to the incomplete HF arcs. The electrode performances are thus evaluated by $ASR_{electrode} = ASR_{total} - R_{el}$, where $ASR_{total}$ is the total area specific resistance of the cells (largest real part of the impedance) and $R_{el}$ is the calculated electrolyte resistance for half the electrolyte thickness. $R_{el} = l_{el} / \sigma_{CGO}$, where $l_{el}$ is half the electrolyte thickness and $\sigma_{CGO}$ is the electrolyte conductivity calculated from $\sigma_{CGO} \cdot T = 1.09 \cdot 10^5 \cdot \exp(-0.64\ eV/(k_B T))$ S·K/cm, which implies $R_{el}$(300 µm, 600 °C) = 1.2 Ω cm². In this way the HF arc is included in the results of $R_p$. Due to the large values of $R_p$ this procedure only give rise to a very small uncertainty on the determination of $R_p$. Standard impedance

fitting with equivalent circuit elements would not be feasible as the HF arcs are too incomplete. For $T_{test} = T_{max} = 600$ °C in air we thus get $ASR_{electrode}$(CGO: STF00) = 6.3 Ω cm$^2$ and $ASR_{electrode}$(CGO: STF10) = 6.4 Ω cm$^2$.

Effect of Sintering Temperature on Electrode Performance

Figure 5b shows Nyquist plots at a test temperature of 600°C after different sintering temperatures between $T_{max}$ = 600-1000 °C for a symmetric cell with CGO backbone infiltrated with STF00. The performance of the cell is observed to be strongly dependent on sintering temperature. The performance is best at $T_{max}$ = 600 °C and decreases with increasing $T_{max}$. The optimal sintering temperature is a balance of sufficient phase formation of the catalytically active phase and microstructure. Sintering at higher temperatures increases particle sizes as previously observed but on the other hand, the perovskite phase is not present or only present in small amounts at low sintering temperatures. Furthermore the amount of $SrCeO_3$ may also increase with increasing sintering temperature. From Figure 5b the ASR is seen to increase strongly at $T_{max} \geq 900$ °C, which may be explained by significant infiltrate particle growth and the increased tendency to form $SrCeO_3$ at elevated temperatures.

Impregnation of Electronically Conductive LCN60/CGO Backbone with STF10

Because of the indications of poor electronic conductivity in the impregnated CGO backbones electronically conductive LCN60/CGO backbones were impregnated. STF10 was chosen as infiltrate as it showed the best performance in the impregnated CGO backbones. Impedance results for impregnated and non-impregnated backbones of LCN60/CGO, sintered and tested at 600 °C in air, are presented in Figure 6. The measurements were conducted in the frequency range 0.06 Hz – 100 kHz, since no high-frequency arc was encountered, which is attributed to better electronic conductivity in the electrode. The LCN60/CGO cell without infiltrate exhibits a performance of $ASR_{electrode} = R_p$ = 8.7 Ω cm$^2$ at 600 °C in air. The performance has been evaluated by using the data points measured at 100 kHz and 0.06 Hz.

A large variation in $R_s$ for some of the LCN/CGO cells has been observed. As seen from Figure 6 two of the cells exhibit a very high series resistance, which is attributed to contact resistances at the electrode-electrolyte interface. It is although expected that impregnation decreases $R_s$ significantly for the cells with bad contacting. Values of $ASR_{electrode}$ have although proved highly reproducible.

Figure 6 shows a significant improvement of the electrode performance when impregnating with STF10. $ASR_{electrode}$ of the cell infiltrated 4 times with STF10 has been measured to 0.34 Ω cm$^2$ and for the cell impregnated 10 times with STF10, $ASR_{electrode}$ = 2.7 Ω cm$^2$, corresponding to electrode performance improvements of 25 and 3 times, respectively, compared to the non-impregnated cell. Hence, the optimal number of impregnations is expected to be closer to 4 than 10 and the number of impregnations has a large impact on the electrode performance. Previous studies by Samson *et. adf.* impregnation of a CGO backbone with LSC40 show performance variations of no more than a factor of 2 when impregnating 6, 9 and 12 times and an optimal performance at 9 impregnations [9].

The differences between the present study and that of Samson *et. al.* are expected to be caused by the content of the catalytically active LCN60 in the electrode backbone in this work. For illustration of the catalytic activity, LCN60/CGO electrodes with optimized microstructure exhibit a performance of $ASR_{electrode}$ = 0.4 Ω cm$^2$ at 600 °C in air, thus almost as good as the best impregnated LCN60/CGO electrodes in the present study [11]. The LCN60 particles get increasingly blocked with the number of impregnations, which reduces the gas accessibility to the surface and thus the oxygen reduction activity of the LCN60. This hypothesis would mean that the net catalytic activity of the STF infiltrate is less than that of LCN60. This may be due to the presence of secondary phases or less optimistic materials parameters than reported in literature. Further investigations would have to be carried out to confirm this.

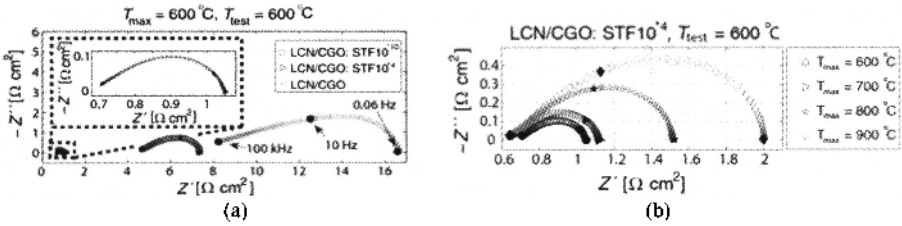


Figure 6. Nyquist plots showing (a) impedance measurements of LCN60/CGO symmetric cells impregnated with STF10 10 times (☆), 4 times (▷) and without infiltrate ( · ). The cells were sintered and tested at 600 °C in air. (b) Nyquist plots showing performance variation with in-situ sintering temperature ($T_{max}$) at 600 °C in air for a STF10 impregnated symmetric cell with LCN60/CGO backbone.

The performance impact of sintering temperature is illustrated in Figure 6b. The electrode performance is best at a sintering temperature of 600 °C. Increasing the sintering temperature decreases the electrode performance, although not nearly with as large a factor as observed for the impregnated CGO backbone. Again, this is explained by the presence of the catalytically active LCN60 phase, in which the particle sizes are only slightly affected by increasing the sintering temperature from 600-900 °C and thus do not imply a performance decrease. However, the significant performance decrease with increased $T_{max}$ shows that the infiltrated STF10 must contribute significantly as a catalyst for the electrochemical reduction of $O_2$.

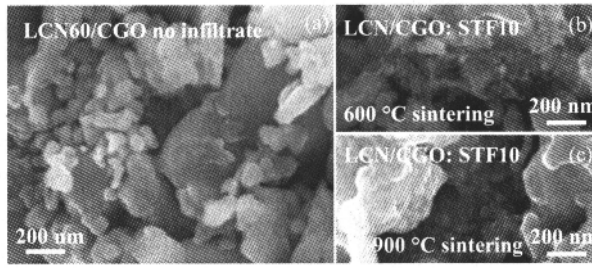


Figure 7. SEM photos of LCN60/CGO electrode backbones (a) without infiltrate, (b) with STF10 sintered at 600 °C and (c) with STF10 sintered at 900 °C.

Micrographs of a non-impregnated LCN60/CGO backbone are shown in Figure 7. The non-impregnated backbone in Figure 7a shows large particles with sizes ~200 nm and smaller particles with sizes < 100 nm due to a different particle size distribution for the LCN60 and CGO phases. After 4 impregnations with STF10 and sintering at 600 °C the infiltrate can be seen as particles smaller than those in the backbone, see Figure 7b. Sintering at 900 °C entails agglomeration to particles of sizes ~50 nm as shown in Figure 7c. As previously observed the particles seem to form a very low contact angle on the backbone particles.

The electrode performances of STF10 impregnated CGO and LCN60/CGO backbones and a non-impregnated LCN60/CGO backbone are compared in an Arrhenius type plot in Figure 8. The ASR of the non-impregnated LCN60/CGO backbone varies only slightly with $T_{max}$, showing limited degradations, since the cells have already been sintered at 1000 °C during the fabrication process [11].

The performance of the STF10 impregnated CGO backbone changes remarkably little with increased $T_{max}$ in the range 500-800 °C compared to the STF10 impregnated LCN60/CGO backbone as well as other cells that have been tested in this study.

The activation energies shown in Figure 8 have been calculated for the data points corresponding to $T_{max}$ = 800 °C. The non-impregnated LCN60/CGO electrode with $E_a$ = 70.9 kJ/mol performs better than the STF10 impregnated CGO backbone at $T_{test}$ > ~700 °C but worse at lower temperatures. The relatively low activation energy of the impregnated CGO backbone is believed to be due to the large influence of electronic and oxygen vacancy conduction limitations on the electrode performance. These processes are less activated with temperature, which can be exemplified by comparing $E_a$ = 61.8 kJ/mol for vacancy conduction in CGO and an activation energy for a thin film electrode of STF50 of $E_a$ = 173.7 kJ/mol. The performance of the thin film electrode is largely dominated by the reduction process of oxygen. [120]

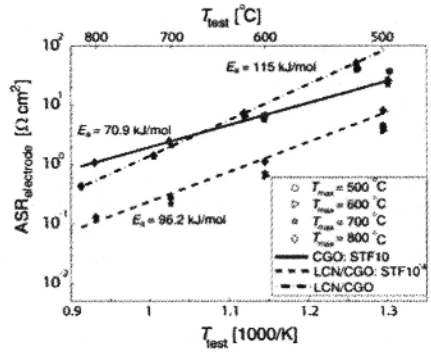


Figure 8. The electrode performance, $ASR_{electrode}$, as function of temperature. The performance has been plotted at various temperatures with a symbol showing the in-situ sintering temperature ($T_{max}$ = 500-800 °C) of the cell. An Arrhenius fit to the data obtained for $T_{max}$ = 800 °C has been included.

The performance of the best LCN60/CGO backbones impregnated with STF10 is still an order of magnitude lower than that of LSC40 impregnated CGO backbones even though the electronic conductivity issues to some degree have been solved by introducing the electronically conducting LCN60/CGO backbone. This may have several explanations; the net catalytic activity and net conductivities of the STF infiltrate are not expected to be very good, the STF particles constitute a significantly reduced surface area compared to the LSC40 infiltrate in the study by Samson et al and the suspected infiltrate-backbone reactions to form $SrCeO_3$ can cause a strong impediment of oxide ion transport from the infiltrate to the CGO backbone. [9]

## SUMMARY

$SrTi_xFe_{1-x}O_{3-\delta}$ (STF) was evaluated as potential material in solid oxide fuel cell (SOFC) cathodes by impregnating $Ce_{0.9}Gd_{0.9}O_{2-\delta}$ (CGO) backbones with the compositions x = 0; 0.1; 0.2; 0.3; 0.4 and 0.5. On average the best performance was observed for STF10 impregnated CGO backbones with an electrode area specific resistance (ASR) of 6.4 Ω cm² at 600 °C in air. A large part of the ASR is attributed to poor electronic conductivity of the electrode and possibly formation of the highly resistive phase $SrCeO_3$.

$CGO/LaCo_{0.4}Ni_{0.6}O_{3-\delta}$ (LCN60) electrodes 50/50 wt% with high electronic conductivity were impregnated with STF10 (x = 0.1) and showed an ASR of 0.34 Ω cm² at 600 °C in air, which is an

improvement of 25 times compared to the non-impregnated electrode with an ASR of 8.7 $\Omega$ cm$^2$. It is suspected that the temperatures needed for formation of STF are too high for compatibility with the impregnation technique, which implies extensive formation of secondary phases. Although no precise conclusion for the potential of STF as cathode material in SOFC has been stated, the following has been found:

- If implications of the high thermal expansion coefficient (TEC) can be overcome, STF compositions with a high content of iron such as STF10 show the most interesting properties.
- The formation of STF from strontium and iron nitrate and titanium lactate is accompanied with formation of several unwanted secondary phases, even when heating to 1100 °C.
- STF infiltrate and CGO may react to form an isolating $SrCeO_3$ phase at high temperatures.
- STF infiltrate forms a coating on CGO instead of the wanted high-surface area distribution of infiltrate particles.
- STF infiltrate sintered in-situ at 500-900 °C does not provide the desired combination of high oxygen surface exchange, high electronic conductivity and good ionic conductivity.

ACKNOWLEDGEMENTS

Special thanks to Søren Primdahl (Topsoe Fuel Cell A/S) for academic input and discussion of the results in this work, Per Hjalmarsson (Risoe DTU) for provision of LCN60/CGO and to Alfred Samson (Risoe DTU) for provision of CGO backbones and assistance in the experimental work carried out. Thanks to Carsten Gynther (Risoe DTU) for assistance with TG measurements.

REFERENCES

[1]Jung, W., Harry L. Tuller. *Solid State Ionics*, **180**, 843-847 (2009).
[2]Rothschild, A., W. Menesklou, H. L. Tuller, E. Ivers-Tiffée. *Chem. Mater.*, **18**, 3651-3659 (2006).
[3]Patrakeev, M. V., I. A. Leonidov, V. L. Kozhevnikov, V. V. Kharton. *Solid State Sc.*, **6**, 907-913 (2004).
[4]Ullmann, H., N. Trofimenko, F. Tietz, D. Stöver, A. Ahmad-Khanlou. *Solid State Ionics*, **138**, 79-90 (2000).
[5]Brixner, L. H. *Mat. Res. Bull.*, **3**, 299-308 (1968).
[6]Kharton, V. V., et al. *Solid State Ionics*, **133**, 57-65 (2000).
[7]*SurfaceNet*. http://www.surfacenet.de/html/strontium_titanate.html (06. December 2011).
[8]Singhal, S. C., K. Kendall. High Temperature Solid Oxide Fuel Cells: Fundamentals, Design and Applications, chapter 4 & 5. *Elsevier Advanced Technology*, Oxford, 2003.
[9]Samson, A., M. Søgaard, R. Knippe, and N. Bonanos. *J. Electrochem. Soc.*, **158 (6)**, 1-10 (2011).
[10]Nicholas, J. D., S. A. Barnett. *J. Electrochem. Soc.*, **157 (4)**, B536-B541 (2010).
[11]Hjalmarsson, P., M. Mogensen. *J. Power Sources*, **196**, 7237–7244 (2011).
[12]Gharbage, B., F. Mandier, H. Lauret, C. Roux, T. Pagnier. *Solid State Ionics*, **82**, 85-94 (1995).
[13]Wang, H. B., J. F. Gao, D. K. Peng, G. Y. Meng. *Mat. Chem. Phys.*, **72**, 297-300 (2001).
[14]Takeda, Y., et al. *J. Solid State Chem.*, **63**, 237-249 (1986).
[15]Majid, A., J. Tunney, S. Argue, M. Post. *J. Sol-Gel Sc. and Tech.*, **32**, 1-3, 323-326 (2004).
[16]Iwahara, H., T. Esaka, H. Uchida, N. Maeda. *Solid State Ionics*, **3/4**, 359-363 (1981).
[17]Nag, A., T. R. N. Kutty. *Royal Society of Chemistry*.
http://www.rsc.org/suppdata/jm/b2/b207756f/b207756f.pdf (11. December 2011).
[18]Huang, Y., J. M. Vohs, R. J. Gorte. *Electrochem. and Solid-State Let.*, **9 (5)**, A237-A240 (2006).
[19]Bidrawn, F., S. Lee, J. M. Vohs, R. J. Gorte. *J. Electrochem. Soc.*, **155 (7)**, B660-B665 (2008).
[20]Steele, B. C. H. *Solid State Ionics*, **158 (6)**, 95-110 (2000).